Learning Local Shape and Appearance for Segmentation of Knee Cartilage in 3D MRI *

Soochahn Lee[1], Hackjoon Shim[2], Sang Hyun Park[1],
Il Dong Yun[3], and Sang Uk Lee[1]

[1] ASRI, SoEECS, Seoul Nat'l Univ.,
redhouse@cvl.snu.ac.kr,shpark@cvl.snu.ac.kr,sanguk@ipl.snu.ac.kr
[2] BK21 Research Division for Information Technology, Seoul Nat'l Univ.,
hjshim@diehard.snu.ac.kr
[3] Dept. of Digital Information Eng., Hankuk Univ. of Foreign Studies,
yun@hufs.ac.kr

Abstract. We present experimental evaluation of a new fully-automatic method for accurate knee cartilage segmentation based on 40 test and 60 training images of the **SKI10** set. The method is comprised of three main steps: bone segmentation, bone-cartilage interface (BCI) classification, and cartilage segmentation. For cartilage segmentation, reference patches are extracted from training images by comparing the position and appearance of sampled local patches on the BCI. These reference patches provide specific local shape and appearance information to segment each patch by graph cuts using detailed local region and boundary cues. The segmentations of all patches are combined to obtain the whole cartilage segments. The average score was slightly lower than the 75 points of manual segmentation by expert raters at 65 for femoral and 68 for tibial cartilage demonstrating the accuracy of our method.

1 Introduction

Accurate segmentation of cartilage in 3-D magnetic resonance (MR) images for quantitative assessment of volume/thickness is crucial for studying and diagnosing osteoarthritis (OA) of the knee, a leading cause of disability in aged population. Despite the necessity to further research, automatic segmentation of knee cartilage is extremely difficult due to inhomogeneities, small size, low tissue contrast, and shape irregularity. Furthermore, subdivision into femoral/tibial/patellar components is also exceedingly hard due to overlapping intensity distributions and ambiguous boundaries.

Many previous methods have circumvented these difficulties based on sparse user annotations. Various semi-automated segmentation techniques applying active shape models [1], b-spline snakes [2] and graph-cuts [3] have been proposed.

* This research was supported by Basic Science Research Program through the National Research Foundation of Korea(NRF) funded by the Ministry of Education, Science and Technology (20090074888 and 20100012006)

Although these techniques provide significantly better efficiency than manual boundary delineation, they still require careful annotations.

Recent research has been focused on the development of a fully-automatic method without the need for any user interaction. The method proposed by Folkesson et al. [4] uses k-nearest neighbor (k-NN) classifiers to classify cartilage and non-cartilage voxels. Classifiers corresponding to features such as voxel position, raw and Gaussian smoothed intensities, and intensity derivatives are trained. However, the classifiers cannot fully represent cartilage characteristics due to limited discriminative power.

More sophisticated methods by Fripp et al. [5] and Yin et al. [6] are both based on a framework comprised of pre-segmentation of knee bones and segmentation of the corresponding cartilage compartment. Both methods construct a mesh model of each bone surface and identify vertices on the bone-cartilage interface (BCI) by training. Fripp et al. [5] expand this model to explicitly construct a dense BCI and then determine outer cartilage boundary by examining the intensity profile of a constrained local region in the direction normal to the BCI. Yin et al. [6] apply an optimal multi-surface segmentation method [7] to constrain segmentation so that the geometric relation between bone and cartilage reflects trained characteristics. For both methods, the focus is more on global characteristics such as intensity mean and variance or estimated thickness.

The method of this paper emphasizes more on local characteristics by determining the relevant local shape and appearance information from atlas images. By examining relevant local regions in various images from the atlas set and incorporating flexible region and boundary cues, our method is able to explicitly determine the appropriate local characteristics to enhance segmentation performance.

Following the methods of Fripp et al. [5] and Yin et al. [6], the overall framework is comprised of three main steps: bone segmentation, BCI classification, and cartilage segmentation. Sec. 2 provides an overview while Sec. 3, 4, and 5 provide describe each process specifically. Experimental results are given in Sec. 6 and the paper is concluded in Sec. 7.

2 Overview

Due to the relatively simple shapes of knee bones and the high contrast at the BCI, bone segmentation and BCI classification are generally easier tasks than direct cartilage segmentation. Furthermore, the BCI represents a significant portion of the cartilage boundary and provides a valuable basis in identifying the remaining boundary due to the thin plated shape of cartilage. Thus we first segment bone compartments, determine the BCI, and then segment cartilage.

A flowchart summarizing each subprocess is presented in Fig. 1. We assume that a training set Ω comprised of N cases is established. Each data $\omega_n \in \Omega$, $n = 1, \cdots, N$, is comprised of the MR image $\mathcal{I}_{\omega_n}$, cartilage label mask $\mathcal{C}_{\omega_n}$, and bone label mask $\mathcal{B}_{\omega_n}$. Bone-cartilage interface points BCI_{ω_n} can be computed from $\mathcal{C}_{\omega_n}$ and $\mathcal{B}_{\omega_n}$. The set of all $\mathcal{I}_{\omega_n}$, $\mathcal{C}_{\omega_n}$, $\mathcal{B}_{\omega_n}$, and BCI_{ω_n} over the training set

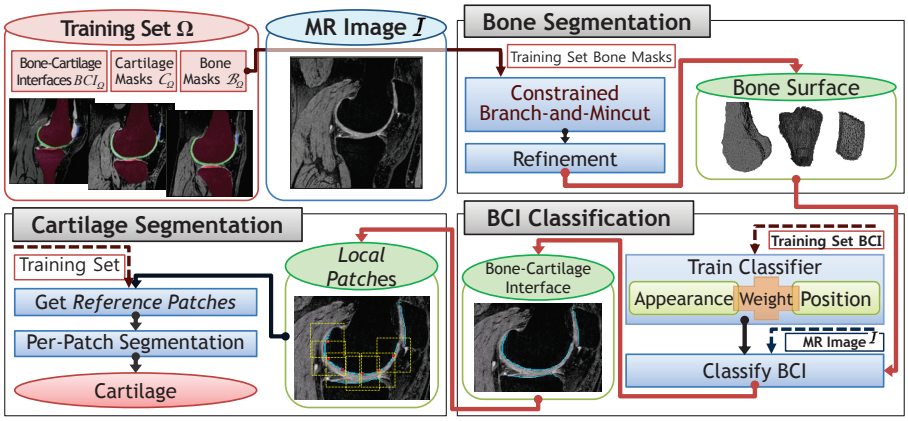

Fig. 1. Flowchart of the proposed method.

Ω are denoted as $\mathcal{I}_\Omega$, $\mathcal{C}_\Omega$, $\mathcal{B}_\Omega$, and BCI_Ω, respectively. After pre-segmentation of bone compartments from the input MR image $\mathcal{I}$ using B_Ω as bone shape templates, voxels on the bone surface are classified into BCI BCI_I and non-BCI BCI_I^c based on position and local appearance.

For cartilage segmentation, a set of *anchor points* $v_i^a \in BCI_I^a \subset BCI_I$, $i = 1, \cdots, |BCI_I^a|$ are established by stratified sampling of the BCI voxels. Corresponding local patches $\mathbf{v}_i^a$ centered at each anchor point are then defined, and *reference patches* comprised of corresponding patches from $\mathcal{I}_{\omega_n}$, $\mathcal{C}_{\omega_n}$, and $\mathcal{B}_{\omega_n}$ are determined from Ω. Assigned reference patches, which contain the relevant information to segment $\mathbf{v}_i^a$, are collectively used as region and boundary priors to enable accurate local segmentation of cartilage. Details of each subprocess will be given in the following sections.

3 Bone Segmentation

We apply the method of Lee et al. [8] for bone segmentation. As described in Fig.1, a modified version of the recently proposed branch-and-mincut method [9], termed *constrained branch-and-mincut*, is applied to each bone compartment based on mean shapes constructed from $\mathcal{B}_\Omega$ for coarse segmentation of $\mathcal{I}$.

The branch-and-mincut method [9] is based on graph cuts [10], but assumes an additional variable representing a set of non-local prior, such as a set of shape priors, in the optimization process. To avoid brute force comparison of results obtained based on different shapes to determine the optimal one, branch-and-bound tree search is applied by defining a lower bound of energy for a given set of shape priors. This lower bound energy is computed by min-cut [11], hence the name of the method.

In our bone segmentation process, the original image based method is extended to 3-D medical images, substituting pixels by voxels. To further enhance

efficiency, criteria to prune nodes with corresponding subsets unlikely to contain the optimal shape prior is added to branch-and-bound tree search. For this constrained branch-and-mincut, we use the mean bone shape, computed by aligning all $\mathcal{B}_\Omega$ and then averaging and thresholding all voxels, at different translational positions as the set of shape priors. The approximate shape and position of the bone in $\mathcal{I}$ is given as the output.

This intermediate segmentation is then refined by determining both the optimal segmentation and the optimal individual bone mask among $\mathcal{B}_\Omega$ to obtain the final bone segmentation.

4 Bone-Cartilage Interface Classification

From the bone segmentation we classify voxels on the bone surface as BCI and non-BCI based on position and local appearance. A combined classifier representing both distance and appearance is constructed by training separate classifiers and learning the distribution of weights used to average them.

The positional classifier is based on the ratio of average minimum distances of the current voxel from BCI_Ω and BCI^c_Ω. We compute and average separate distance transforms [12] D_{BCI} and D_{BCI^c} from each BCI_{ω_n} and $BCI^c_{\omega_n}$. Before averaging the distance transforms, affine registration is done by ICP [13] to align corresponding bone compartments. The input image bone surface is similarly aligned and for each voxel v on the bone surface, probability of it being on the BCI based on position is defined as $P_{pos}(v \in BCI_I) = 1 - \frac{D_{BCI}(v)}{D_{BCI}(v)+D_{BCI^c}(v)}$.

For appearance, we construct bags of image patches Θ_{BCI} and Θ_{BCI^c} representing the respective local appearance of BCI_Ω and BCI^c_Ω. Specifically, from all voxels in BCI_Ω and BCI^c_Ω, an image patch is extracted from I_Ω. Principal component analysis (PCA) and clustering is applied to reduce the patch dimensions and the number of the patches. Then for each voxel v on the bone surface appearance based probability is defined as $P_{app}(v \in BCI_I) = 1 - \frac{A_{BCI}(v)}{A_{BCI}(v)+A_{BCI^c}(v)}$ where $A_{BCI}(v)$ is the average Euclidian distance between the PCA coefficients of image patch centered on v and those of the k-nearest neighbors (k-NN) in Θ_{BCI}. Here, distances between image patches are defined as normalized cross correlation (NCC).

Finally, we construct a per-voxel weight map by weighing the consistency of $P_{pos}(v_)$ and $P_{app}(v)$ for voxels v on the surface of B_Ω. The position and appearance weight are defined as $w_{pos} = \frac{P_{pos}}{P_{pos}+P_{app}}$ and $w_{app} = 1 - w_{pos}$, respectively. Since voxels on bone surfaces are sparse, diffusion is applied to make the weight map dense.

5 Cartilage Segmentation

Due to the thin structure of cartilage, a region of interest (ROI) can be designated based on the BCI. The main idea of our method is to designate this ROI as a collection of separate local image patches, and use relevant *reference patches* from

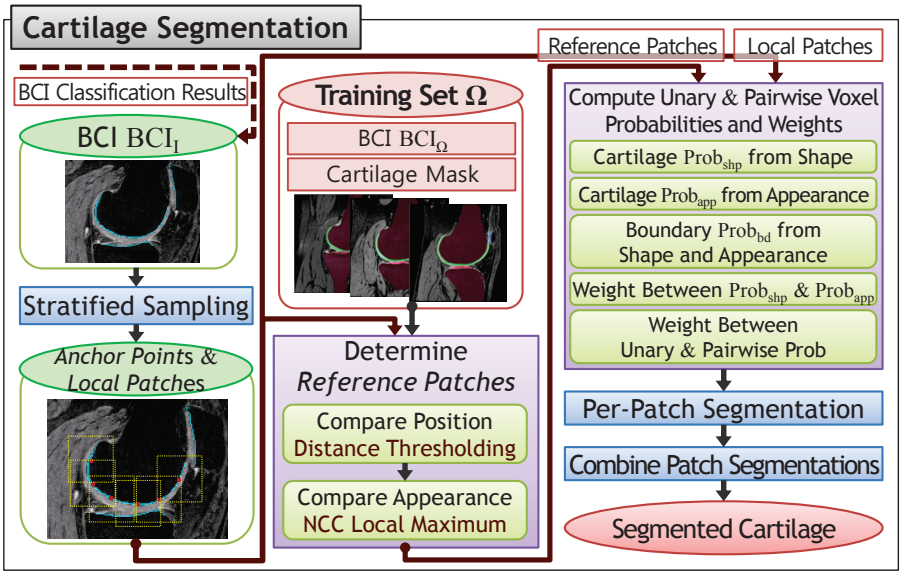

Fig. 2. Flowchart of the proposed BCI classification process.

Ω to compute region probability of cartilage/non-cartilage for single voxels and boundary probabilities for neighboring voxel pairs. Based on these probabilities, graph cut [10] is applied for segmentation of each patch. A flowchart summarizing our cartilage segmentation method is presented in Fig 2.

Stratified sampling is first applied to BCI_I to obtain evenly distributed *anchor points* $v_i^a \in BCI_I^a$ which will be the center of each local patch $\mathbf{v}_i^a$. Next, corresponding *reference patches* for each $\mathbf{v}_i^a$ is determined from the training set Ω. For each $\mathbf{v}_i^a$, only voxels among $v \in BCI_{\omega_n}$ within a distance threshold θ_d are extracted for each ω_n. The NCC between $\mathbf{v}_i^a$ and the local image patches centered at the extracted voxels are computed, and the patch with maximum NCC is determined. If the NCC value of this patch is above threshold θ_{NCC}, it is designated as a reference patch for $\mathbf{v}_i^a$.

We construct a Markov random field (MRF) for actual segmentation. The graph cut [10, 11] technique determines the optimal configuration for the vector of labels $\mathbf{x}$ comprised of binary labels x_v for each voxel v in set $\mathcal{V}$ that minimizes the following energy function of the MRF:

$$E(\mathbf{x}) = \sum_{v \in \mathcal{V}} \phi(x_v) + \lambda \sum_{u,v \in \mathcal{E}} \psi(x_u, x_v). \tag{1}$$

x_v is either foreground (FG) or background (BG), and in this case FG and BG represent cartilage and non-cartilage tissue, respectively. $\phi(x_v)$ and $\psi(x_u, x_v)$ represent functions of unary potential for v and pairwise potential for the neighboring voxel pair $(u, v) \in \mathcal{E}$, respectively.

The unary probabilities are computed as the weighted average of separate probabilities based on the reference shape and appearance models. Following the method of Bai et al. [14] shape priors are emphasized for local regions with low gradients along the cartilage boundary, while appearance priors are emphasized regions with high gradients. Specifically, for each voxel $v \in \mathbf{v}_i^a$, an intensity based FG probability is defined as $P_i(v) = \frac{P(v|H_{FG})}{P(v|H_{FG})+P(v|H_{BG})}$ where H_{FG} and H_{BG} are histograms constructed by voxels of $\mathbf{v}_i^a$ respectively using corresponding labels from the cartilage labels of reference patches $\mathcal{C}_i^a$. Then, the confidence of the intensity probability P_i is measured as:

$$f_c = 1 - \frac{1}{\sum\limits_{v \in \mathbf{v}_i^a} d_c(v)} \sum_{v \in \mathbf{v}_i^a} d_c(v)\, |\mathcal{C}^a(v) - P_i(v)|, \tag{2}$$

where $d_c(v)$ represents the distance to the FG/BG boundary of $\mathcal{C}_i^a$. This value increases as P_i agrees more with reference labels close to the boundary and is used to control the weight $f_s(v)$ between enforcing appearance probability P_i and reference labels $\mathcal{C}_i^a$. The combined FG probability is now defined as $P(v = FG) = (1 - f_s(v))P_i(v) + f_s(v)\mathcal{C}_i^a(v)$. Since there may be multiple reference patches for $\mathbf{v}_i^a$, FG probabilities based on multiple reference patches are averaged and the potential is defined as $\phi\,(x_v) = -\log\left(\frac{1}{R}\sum\limits_{r \le R} P_r\right)$, where R is the number of reference patches.

We further use reference patches to model the local gradient distribution of cartilage boundary and compute pairwise probabilities. Specifically, we construct separate histograms H_{FF}, H_{BB} and H_{FB} of intensity differences $|I(u) - I(v)|$ for $(u = FG, v = FG)$, $(u = BG, v = BG)$, and $(u = FG, v = BG)$ voxel pairs, and define boundary probability as

$$\begin{aligned} P_{bd}(u = FG, v = BG)) = P(u = FG)\frac{P(u, v|H_{FB})}{P(u, v|H_{FB}) + P(u, v|H_{FF})} \\ + P(u = BG)\frac{P(u, v|H_{FB})}{P(u, v|H_{FB}) + P(u, v|H_{BB})}. \end{aligned} \tag{3}$$

This represents the weighted average of relative probabilities of the voxel pair being on the boundary compared to both being on the foreground or background. P_{bd} values based on different reference patches are once again averaged and $\psi\,(x_u, x_v) = -\log\left(\frac{1}{R}\sum\limits_{r \le R} P_{bd}\right)$.

Finally, graph cut is applied to each local patch for per-patch segmentation, and these segmentations are combined to obtain the final cartilage segments.

6 Experimental Results

For efficiency, we apply a multi-resolution framework where our method is first performed on data downsampled by a factor of 2, and then upsampled. parameters applied for given results as follows: $k = 3$ for A_{BCI}, $\theta_d = 7mm$, $\theta_{NCC} = 0.6$,

and local patch sizes were fixed to $(20, 20, 10)$. Classifying each BCI compartment takes 10-20 seconds, while each cartilage segmentation takes 1-3 minutes depending on the size of bone and number of extracted reference patches. Running time for bone segmentation varies much depending on the difficulty of the image. We note that all experiments were run on a 2.40GHz core2 Quad CPU with 2GB RAM with unoptimized code.

Table 1 presents the accuracy of our method for the 40 test cases. Here AvgD and RMSD denote the average and RMS surface distance, respectively, while VOE is the volumetric overlap error and VD indicates the volumetric difference. Scr denotes the score computed by combining all measures. The score for manual segmentation results by expert raters was defined as 75 points. This score is used as a benchmark of performance, along with the 100 points representing segmentations exactly matching the reference.

The average score for the bone segmentation method were low for both the femor and the tibia, being only 26 and 49 points, respectively. This low score of the bone segmentation results were mainly due to large inaccuracies in the upper regions for the femor and lower regions for the tibia. In many cases, the bone shapes from the training set used as shape priors were severed at image boundaries which led to similarly severed segmentations. Moreover, due to low gradient and similar intensity distributions of bone and other tissue, accurate delineation of the bone boundary at these regions. The results on sample cases shown in Fig. 3 demonstrates this tendency. However, we can also see that segmentation results at the BCI were accurate, which is sufficient for our method where bone segmentation is essentially a preprocessing step for cartilage segmentation.

We can see that despite the low score of bone segmentation results, our cartilage segmentation method performed well, giving average scores of 65 for femoral cartilage and 68 for tibial cartilage, both close to 75 points. Despite high scores, the score variance were also high for both cartilages at 15 and 18, respectively. This inconsistent performance is mostly due to the direct referencing characteristics of the method. If there are few cases similar to the input image in the training data, the informative power of the reference images drops significantly. Also, we can see in Fig. 3 most inaccuracies are localized at peripheral regions of the cartilage, while the method gives more accurate results for central regions, where most of the cartilage function is accountable due to the interaction between the cartilage compartments.

7 Conclusion

We present experimental results of a new fully-automatic method for accurate knee cartilage segmentation based on learned local shape and appearance. Since segmentation is based on local regions, appearance and shape models can be more tailored to represent relative characteristics for different positions. We believe that our method has potential for segmenting pathological cartilage, which is important to facilitate further research on OA. The average score of the method

was 65 for femoral and 68 for tibial cartilage and were slightly lower than the 75 points of manual segmentation by expert raters. We believe that these scores demonstrate the accuracy of our method and support potential clinical application.

References

1. Solloway, S., Hutchinson, C.E., Waterton, J.C., Taylor, C.J.: The use of active shape models for making thickness measurements of articular cartilage from mr images. Magnetic Resonance in Medicine **37**(6) (1997)
2. Kauffmann, C., Gravel, P., Godbout, B., Gravel, A., Beaudoin, G., Raynauld, J.P., Martel-Pelletier, J., Pelletier, J.P., de Guise, J.: Computer-aided method for quantification of cartilage thickness and volume changes using mri: validation study using a synthetic model. Biomedical Engineering, IEEE Transactions on **50**(8) (2003) 978 –988
3. Shim, H., Chang, S., Tao, C., Wang, J., Kwoh, C., Bae, K.: Knee cartilage: efficient and reproducible segmentation of high-spatial-resolution mr images with the semiautomated graph-cuts alogrithm method. Radiology **251**(2) (2009) 548–556
4. Folkesson, J., et al.: Segmenting articular cartilage automatically using a voxel classification approach. IEEE Transactions on Medical Imaging **26**(1) (2007) 106 –115
5. Fripp, J., Crozier, S., Warfield, S., Ourselin, S.: Automatic segmentation and quantitative analysis of the articular cartilages from magnetic resonance images of the knee. IEEE Transactions on Medical Imaging **29**(1) (2010) 55 –64
6. Yin, Y., et al.: Simultaneous segmentation of the bone and cartilage surfaces of a knee joint in 3d. In: Proc. of SPIE Medical Imaging. (2009)
7. Li, K., Wu, X., Chen, D., Sonka, M.: Optimal surface segmentation in volumetric images-a graph-theoretic approach. IEEE Transactions on Pattern Analysis and Machine Intelligence **28**(1) (2006) 119 –134
8. Lee, S., Park, S., Shim, H., Yun, I., Lee, S.: 3-d segmentation of knee bones on mr images by constrained branch-and-mincut. In: Probabilistic Models for Medical Image Analysis, A MICCAI Workshop. (2009)
9. Lempitsky, V., Blake, A., Rother, C.: Image segmentation by branch-and-mincut. In: European Conference on Computer Vision. (2008) IV: 15–29
10. Boykov, Y., Funka-Lea, G.: Graph cuts and efficient n-d image segmentation. IJCV **70(2)** (Feb. 2006) 109–131
11. Boykov, Y., Kolmogorov, V.: An experimental comparison of min-cut/max-flow algorithms for energy minimization in vision. IEEE Transactions on Pattern Analysis and Machine Intelligence **26**(9) (September 2004) 1124–1137
12. Felzenszwalb, P., Huttenlocher, D.: Distance transforms of sampled functions. Cornell Computing and Information Science Technical Report TR2004-1963 (September 2004)
13. Besl, P., McKay, N.: A method of registration of 3-d shapes. IEEE Transactions on Pattern Analysis and Machine Intelligence **14(2)** (1992) 239–256
14. Bai, X., Wang, J., Simons, D., Sapiro, G.: Video snapcut: Robust video object cutout using localized classifiers. ACM Transaction on Graphics **28**(3) (2009)

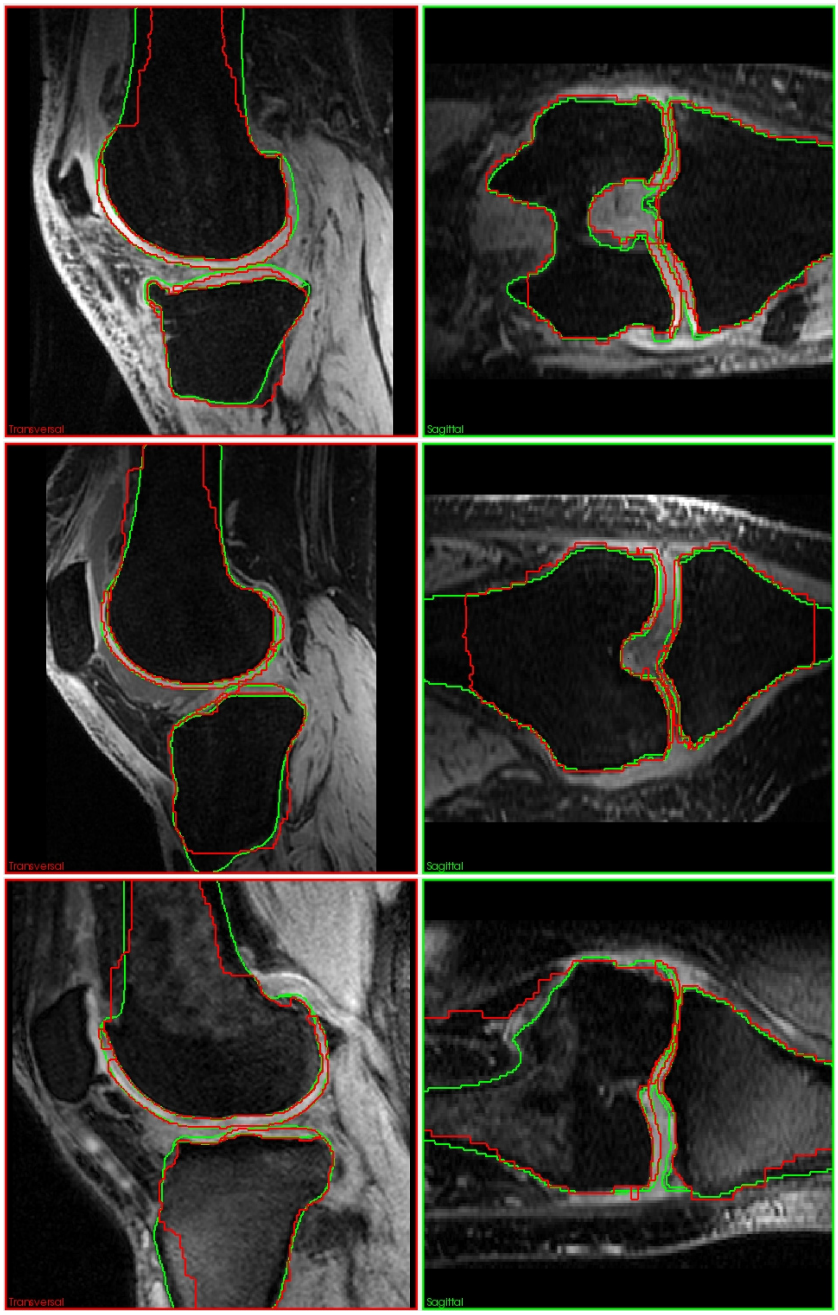

Fig. 3. Different views on selected test cases 8 (top), 16 (center), and 31 (bottom). The outline of the reference segmentation is displayed in green, the outline of the automatic method described in this paper in red.

Img	Femur bone			Tibia bone			Fem. cartilage			Tibial cartilage			Total
	AvgD [mm]	RMSD [mm]	Scr	AvgD [mm]	RMSD [mm]	Scr	VOE [%]	VD [%]	Scr	VOE [%]	VD [%]	Scr	Score
1	0.83	1.41	54	0.81	1.58	41	20.4	10.4	74	41.3	-12.2	63	58.1
2	1.10	1.93	38	1.39	2.72	3	28.8	-19.4	55	27.9	-23.7	48	36.2
3	0.89	1.42	52	0.53	0.83	65	26.1	13.3	67	44.5	26.3	37	55.5
4	1.04	1.76	43	0.54	0.86	64	27.2	14.8	64	21.3	-10.7	73	61.1
5	2.40	4.35	0	0.69	1.09	55	29.3	13.6	65	36.1	-1.8	84	51.0
6	1.25	2.10	31	0.62	1.02	59	28.6	19.0	56	26.3	4.0	83	57.3
7	1.35	2.70	19	0.79	1.27	48	30.0	-9.4	73	32.7	-1.6	85	56.1
8	1.08	1.71	42	0.67	1.27	52	29.8	-16.2	61	37.8	-21.2	49	50.8
9	1.57	3.14	6	0.60	0.97	60	30.1	-17.6	58	36.6	8.7	71	49.0
10	1.39	2.38	23	0.62	1.02	58	40.3	-18.6	53	28.8	-17.2	59	48.3
11	1.85	3.85	0	0.74	1.44	46	26.4	6.9	78	35.2	2.2	83	51.8
12	0.89	1.68	48	0.46	0.77	69	29.4	9.6	72	35.4	11.3	67	64.1
13	1.33	2.47	23	0.75	1.33	48	43.0	33.2	34	34.1	25.7	42	36.9
14	1.00	1.59	47	0.75	1.39	47	37.2	14.1	62	21.4	-1.5	90	61.1
15	0.77	1.43	56	0.56	0.97	61	26.5	24.3	47	29.1	6.8	77	60.5
16	1.38	2.47	22	0.81	1.75	37	34.9	21.7	49	39.6	6.6	74	45.5
17	2.08	3.57	0	0.68	1.03	56	34.5	32.6	37	25.3	1.2	89	45.6
18	1.72	3.27	2	0.56	0.90	63	30.6	12.7	66	26.6	6.2	79	52.8
19	1.12	2.21	33	0.56	1.04	60	29.0	19.5	55	29.2	-2.4	85	58.3
20	1.64	2.80	9	0.61	1.08	58	25.6	5.4	81	35.3	-6.1	76	56.1
21	0.59	0.94	68	1.08	2.51	14	30.3	2.6	84	31.9	-8.2	74	60.0
22	2.88	5.99	0	0.65	1.04	57	25.7	6.0	80	30.9	-3.6	82	54.8
23	1.33	2.79	18	0.72	1.18	52	29.5	4.1	82	48.7	52.2	32	46.0
24	0.97	2.00	41	0.61	0.97	60	30.2	17.6	58	34.5	5.7	77	59.0
25	0.83	1.39	54	0.73	1.27	50	26.3	0.0	90	34.5	0.5	87	70.3
26	1.58	2.54	15	0.77	1.48	44	23.9	12.0	70	34.4	-6.9	75	51.1
27	1.53	2.92	10	0.65	1.05	57	36.4	1.9	83	24.6	-10.7	72	55.7
28	2.26	4.93	0	0.73	1.34	48	38.5	11.9	65	38.0	-28.1	37	37.5
29	0.87	1.40	53	1.47	2.88	0	25.4	-6.4	79	39.2	0.8	84	54.3
30	1.78	3.12	1	0.59	1.04	59	30.5	5.0	80	51.8	-9.0	65	51.3
31	1.94	3.31	0	0.90	1.60	37	28.7	5.4	80	23.7	4.8	83	50.1
32	1.99	3.98	0	0.48	0.72	69	33.2	29.6	38	26.5	23.6	49	38.9
33	1.54	2.73	13	0.70	1.12	54	38.9	12.3	64	45.9	-2.9	78	52.3
34	1.01	1.84	42	0.64	1.35	51	39.6	50.0	36	33.1	28.4	38	41.7
35	1.08	1.92	39	0.58	0.88	62	35.2	7.5	74	37.4	-20.7	50	56.3
36	0.87	1.88	45	0.57	0.99	61	19.0	-0.2	93	24.1	-4.1	84	70.7
37	1.42	2.49	20	1.63	3.33	0	32.9	33.3	38	38.3	43.1	36	23.5
38	1.09	2.24	33	0.48	0.80	68	29.3	10.2	71	23.8	1.3	89	65.3
39	1.72	3.69	2	2.52	5.16	0	36.3	14.7	61	44.1	-9.9	66	32.4
40	1.01	1.98	40	0.72	1.12	53	26.6	13.5	66	50.8	36.2	31	47.7
Avg	1.37	2.56	26	0.77	1.40	49	30.6	10.0	65	34.0	2.3	68	51.9
	±0.50	±1.06	±21	±0.38	±0.84	±19	±5.4	±14.8	±15	±7.9	±17.6	±18	±10.0

Table 1. Results of the comparison metrics and scores for all 40 test cases. AvgD and RMSD are the average and RMS surface distance, respectively, VOE is the volumetric overlap error and VD indicates the volumetric difference.